Low-threshold-current operation of membrane distributed-feedback laser with surface grating bonded on Si substrate

2015 Jpn. J. Appl. Phys. 54 080301

(http://iopscience.iop.org/1347-4065/54/8/080301)

Japanese Journal of Applied Physics **54**, 080301 (2015) **RAPID COMMUNICATION**
http://dx.doi.org/10.7567/JJAP.54.080301

Low-threshold-current operation of membrane distributed-feedback laser with surface grating bonded on Si substrate

Yuki Atsuji[1], Kyohei Doi[1], Takuo Hiratani[1], Daisuke Inoue[1], Jieun Lee[1], Yuki Atsumi[1], Tomohiro Amemiya[2], Nobuhiko Nishiyama[1], and Shigehisa Arai[1,2]

[1]*Department of Electrical and Electronic Engineering, Tokyo Institute of Technology, Meguro, Tokyo 152-8552, Japan*
[2]*Quantum Nanoelectronics Research Center, Tokyo Institute of Technology, Meguro, Tokyo 152-8552, Japan*
E-mail: atsudi.y.aa@m.titech.ac.jp

Received March 6, 2015; accepted May 28, 2015; published online July 1, 2015

A lateral-current-injection (LCI) membrane distributed-feedback (DFB) laser with a surface grating structure (incorporating a slight step) emitting in the 1550 nm wavelength range was fabricated on a Si substrate by the adhesive bonding of benzocyclobutene. For a semiconductor membrane thickness of 158 nm and a surface grating depth of 30 nm, a threshold current of as low as 390 μA, with a corresponding threshold current density of 540 A/cm^2, was obtained for a cavity length of 360 μm and a stripe width of 0.2 μm under a room-temperature continuous-wave (RT-CW) condition.

To date, LSI performance has undergone continuous improvement through downscaling. However, with miniaturization, conventional electrical global wiring structures face limitations due to RC delays, heat generation, and large power dissipation. As a promising solution to these problems, optical interconnections have been studied extensively in recent years. To successfully realize these devices, it was pointed out that their total power dissipation of an optical link should be less than 100 fJ/bit at a signal speed of 10 Gbps.[1)] Therefore, the development of an ultralow-power-consumption semiconductor laser with a small footprint is crucial. In attempts to satisfy these requirements, low-power dissipation operations of vertical-cavity surface-emitting lasers (VCSEL)[2,3)] and photonic crystal lasers[4–6)] have been reported. An alternative candidate also exists in the form of a membrane distributed-feedback (DFB) laser,[7)] with a thin (approximately 150–200 nm) semiconductor core layer sandwiched between low-refractive-index cladding layers such as air, SiO_2, or benzocyclobutene (BCB). The membrane laser is expected to operate with ultralow-power-consumption because of the strong optical confinement in the active layer caused by its high-index-contrast structure.[7–10)] Previously, we demonstrated an optically pumped membrane DFB laser with a low threshold pump power of 0.34 mW under a room-temperature continuous-wave (RT-CW) condition.[11,12)] Furthermore, by introducing a lateral current injection (LCI) structure,[13)] we demonstrated current-injection-type GaInAsP/InP membrane Fabry–Perot (FP) lasers[14,15)] and DFB lasers.[16,17)] Then, the internal quantum efficiency of the GaInAsP/InP membrane FP laser was improved by increasing the top surface thickness of the InP cap layer to 50 nm.[18)] For membrane lasers on a Si substrate, we developed a membrane FP cavity laser under an RT-CW condition[19,20)] and Matuo et al. also demonstrated LCI membrane DFB lasers with direct bonding[21)] at a threshold current of 0.9 mA. Recently, the low-threshold-current (390 μA) RT-CW operation of the GaInAsP/InP LCI membrane DFB laser bonded on a Si substrate has been demonstrated with a relatively long cavity of 360 μm and a very narrow stripe of 0.2 μm.[22)] However, its low threshold property was not well understood because of its poor optical confinement to the active region.

In this letter, we report that the optical confinement factor of the active region of the previously reported GaInAsP/InP membrane DFB laser[22)] was found to be enhanced by the addition of a small step of the stripe geometry, which is the origin of the very low threshold current operation.

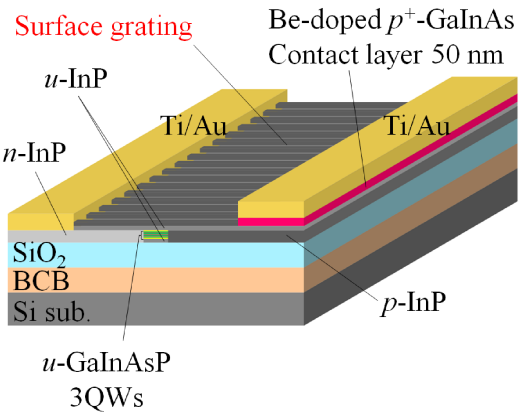

Fig. 1. (Color online) Schematic structure of fabricated LCI membrane DFB laser consisting of surface grating structure.

Figure 1 shows the schematic structure of the fabricated membrane DFB laser with the surface grating structure. The top and bottom cladding layers are air and SiO_2, respectively. The core layer consists of three 1% compressively strained $Ga_{0.22}In_{0.78}As_{0.81}P_{0.19}$ quantum wells (CS-3QWs, 6 nm thick) and 0.15% tensile-strained GaInAsP barriers (TS, 10 nm thick). The total thickness of the core layer, including 50-nm-thick top and bottom undoped-InP surface passivation layers, is 158 nm.[18)] Here, the nondoped InP layer was inserted between a Be-doped ($N_A = 8 \times 10^{18}$ cm^{-3}) p$^+$-GaInAs contact layer [an initial wafer grown by gas-source molecular beam epitaxy (GSMBE)] and a p-InP (Zn-doped, $N_A = 2 \times 10^{18}$ cm^{-3}) layer [second growth by organometallic vapor phase epitaxy (OMVPE)] in order to suppress an optical loss due to the diffusion of the p-dopant from the p$^+$-GaInAs contact layer.

The device was fabricated as follows. An initial wafer consisting of GaInAsP core layers, grown on an n-InP substrate by GSMBE, was used. The LCI structure was then formed through two-step OMVPE selective area regrowth. Firstly, a 7-μm-wide mesa structure was formed using a CH_4/H_2 dry etching process with a SiO_2 mask. n-InP was then selectively regrown on the side of the mesa as a cladding layer. Then, after the etching of the mesa on the n-type cladding layer side, p-InP was regrown in the same manner.

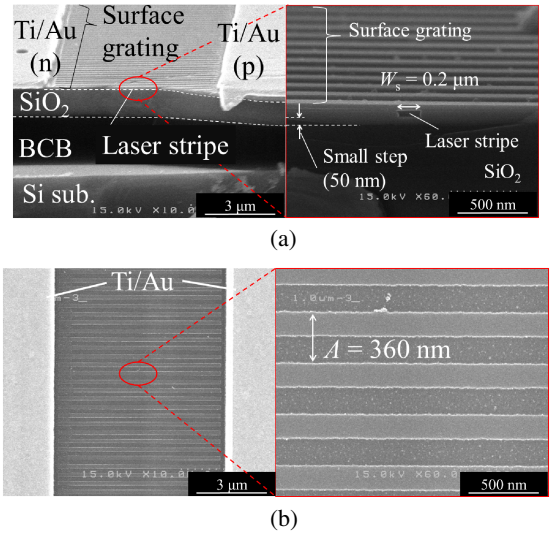

Fig. 2. (Color online) SEM view of fabricated membrane DFB laser: (a) cross-sectional view and (b) top view.

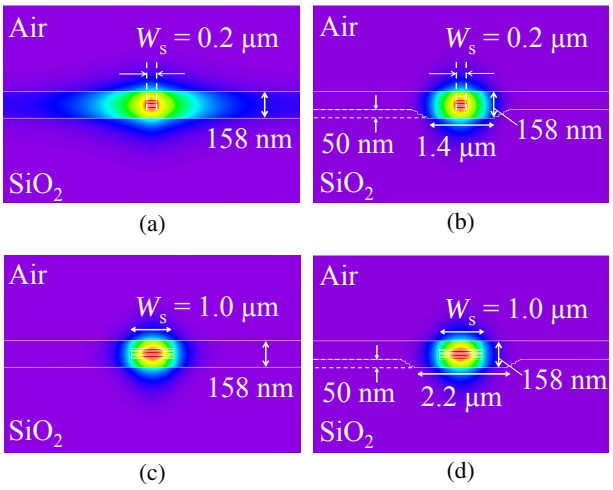

Fig. 3. (Color online) Simulated mode profile of the designed structure for $W_s = 0.2\,\mu m$ with (a) flat structure and (b) selective area regrowth structure, and for $W_s = 1.0\,\mu m$ with (c) flat structure and (d) selective area regrowth structure.

Next, after the deposition of 1-μm-thick SiO_2 and 2-μm-thick BCB layers, the wafer was bonded upside down on a BCB-covered Si host substrate. Compared with direct bonding[21] that required a small surface roughness of less than 1 nm, a high success rate with bonding is expected by using BCB. After bonding, the InP substrate and etch-stop layers were removed by polishing and wet chemical etching. Then, following the removal of the top p^+-GaInAs contact layer (apart from the p-contact section) by wet chemical etching, Ti/Au electrodes were evaporated. Finally, since the equivalent indices n_{eq} of the thick (158 nm) and thin (128 nm) parts of the membrane structure were calculated to be 2.326 and 2.156, respectively, DFB patterns of various periods (between 347.5 and 365.0 nm) with a 2.5 nm step were formed through an electron-beam lithography (EBL) process. The various periods were designed to match the Bragg wavelength to 1560 nm, which was measured from the gain peak of FP lasers fabricated from the same wafer. The depth of the surface grating was 30 nm and the index-coupling coefficient κ was estimated to be approximately $2300\,cm^{-1}$.

Figure 2(a) shows a cross-sectional scanning electron microscopy (SEM) image of the resultant membrane laser. The top and bottom cladding layers of air and SiO_2, and the LCI structure can be seen with a stripe width of $W_s = 0.2\,\mu m$. However, as stated above, the interface between the semiconductor membrane and the SiO_2 cladding is not completely flat: a small step (50 nm high and 0.6 μm wide) exists after the selective area growth of the n- and p-InP cladding layers. Figure 2(b) shows a top-view SEM image of the same sample. As can be seen, the surface grating pattern is clearly visible with a period Λ of approximately 360 nm.

Figure 3 shows the simulated mode profiles of the membrane DFB laser for [(a) and (b)] $W_s = 0.2\,\mu m$ and [(c) and (d)] $W_s = 1.0\,\mu m$, and also for [(a) and (c)] a completely flat structure and [(b) and (d)] a partly thick structure, where simulation was conducted using film mode matching. In the case of $W_s = 0.2\,\mu m$, the optical mode is not well confined within the active region width for the completely flat structure while, for the selective area regrowth structure, it is well confined owing to the InP cladding layer step formed during the selective area growth. A small difference is observed between these structures in the case of $W_s = 1.0\,\mu m$, because the optical mode is almost confined within the active region width.

Figure 4(a) shows the simulated optical intensity distribution profiles along the horizontal direction at the center of the quantum wells in the above-mentioned four cases. As can be seen, the intensity profile has long tails in the case of Fig. 3(a) compared with other three cases; hence, the optical confinement factor of the active region degrades significantly because the difference between the equivalent indices of the active and InP cladding regions is not sufficiently large to confine the optical mode in the horizontal direction.

By varying the stripe width with fixed step height (50 nm) and step width (0.6 μm) conditions at both sides of the active region, the optical confinement factor averaged by the number of quantum wells was calculated for the stripe structure with steps (painted circles) and for a completely flat structure (open triangles), as shown in Fig. 4(b). It can be seen that the optical confinement factor per quantum well of the completely flat structure is almost the same as that of the stripe structure with steps when W_s is sufficiently large, but it decreases sharply when $W_s < 0.6\,\mu m$, and becomes less than half (0.30%/well) of the latter one (0.65%/well) when $W_s = 0.2\,\mu m$. As shown here, the step structure is advantageous in terms of strong optical confinement in a narrow stripe case. The growth rates and times required to obtain the shape in Fig. 2(a) were 23 nm/min and 4.8 min, and 49 nm/min and 2.2 min for p-InP. We think that the step height and width of the flat region can be controlled by choosing the appropriate growth rate and time.

Figure 5(a) shows the light output–current (P–I) and voltage–current (V–I) properties of the membrane DFB laser under an RT-CW condition. The core thickness and cavity length were 158 nm and 360 μm, respectively. As can be seen, a threshold current of 390 μA and an external differential quantum efficiency (DQE) of 3.1% from the front facet were obtained. Considering a membrane FP laser with a cavity length of 440 μm fabricated from the same wafer, which showed a threshold current of 1.4 mA, the reduction in threshold current is considered to be attributable to an

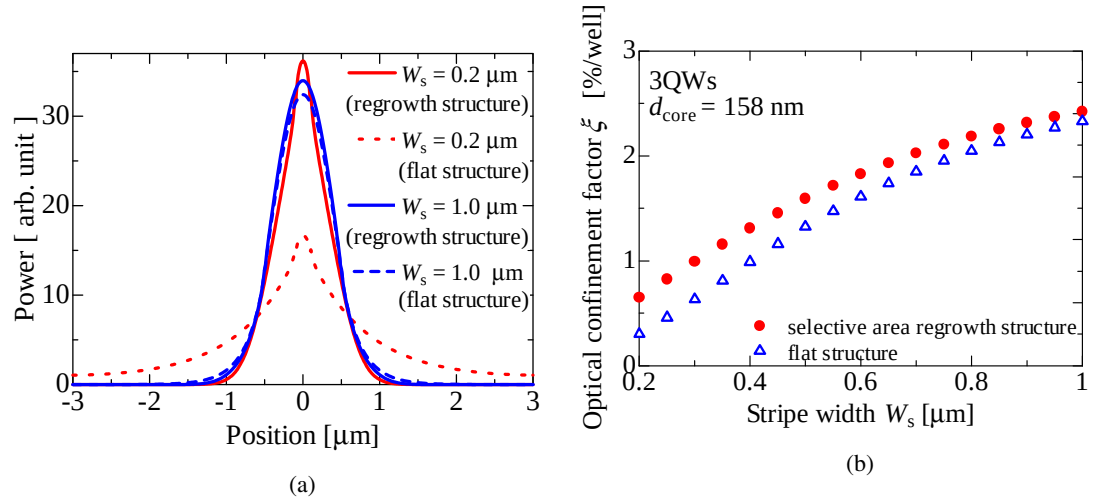

Fig. 4. (Color online) (a) Simulated optical intensity distribution on various structures and (b) optical confinement factor per well as a function of stripe width for flat structure and selective area regrowth structure.

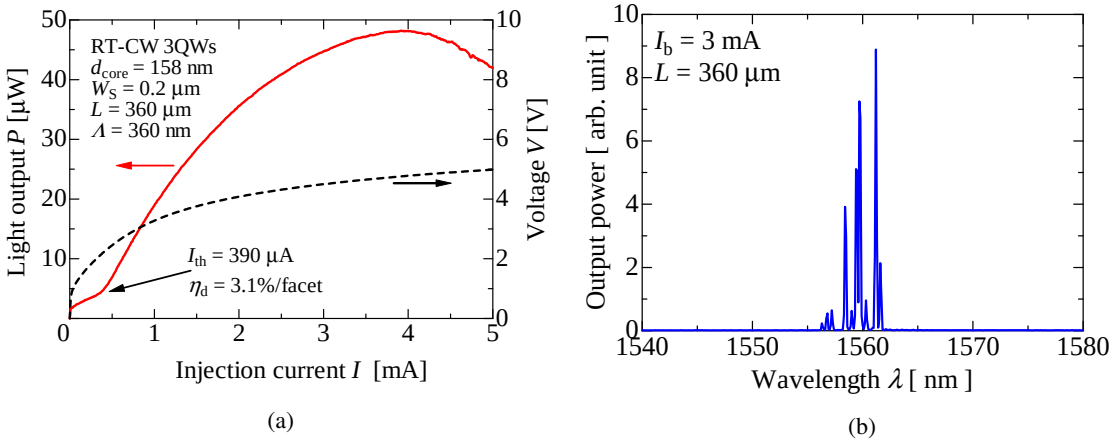

Fig. 5. (Color online) Lasing properties of membrane DFB laser: (a) light output and *V*–*I* characteristics and (b) lasing spectrum.

increase in the reflectivity of the surface grating structure. The poor DQE, however, is considered to be attributable to the strong grating coupling coefficient of $\kappa = 2300\,\mathrm{cm}^{-1}$. On the other hand, the *V*–*I* curve showed a strange tendency in almost all devices obtained from this wafer. Even though the rise-up voltage was found to be 0.8 V, the bias voltage V_B gradually increased with the injection current, and V_B at the threshold was almost 2 V. The differential resistance ($\Delta V/\Delta I$) at an injection current of 3 mA was approximately 350 Ω, which was 7-fold higher than the theoretically estimated value of around 50 Ω. In typical semiconductor lasers, $\Delta V/\Delta I$ should be clamped above the threshold because the stimulated emission becomes dominant, however, the soft rise-up property of the *V*–*I* curve in Fig. 5(a) indicates the existence of strange potential barriers as opposed to a simple p–n junction, and it might affect the leakage current as well as the threshold current but the fraction of the leakage current could not be evaluated. This is an ongoing problem to be solved in the future.

Figure 5(b) shows the lasing spectrum of the membrane DFB laser. Although a single-longitudinal-mode spectrum was not observed in this membrane DFB laser, the mode spacing was not uniform, whereas it was observed to be 0.5 nm for the FP laser (cavity length of 720 μm) fabricated from the same wafer. Furthermore, the stopband was not observed clearly since the stopband width was estimated to be 56 nm, which was too far from the gain peak wavelength (1560 nm) to observe resonant modes on the longer wavelength side of the stopband.

From these values, the effective refractive index (or group index) of the membrane waveguide structure was determined to be $n_{eff} = 3.40$, which seems to be only 10% smaller than that of conventional BH lasers emitting in the 1.5 μm range. On the other hand, $n_{eff} = 3.80$ was obtained for FP lasers with a thicker (220 nm) membrane structure.[20] Since the large discrepancy between the effective index n_{eff} and the equivalent index n_{eq} of the membrane structure was explained for Si-wire waveguides on SOI or air-bridge structures by Sakai et al., which increases with the light wavelength,[23] the discrepancy ($n_{eff} - n_{eq}$) is larger than 1 at the 1.5–1.6 μm wavelength.

Figure 6 shows the cavity length dependences of the threshold currents of the membrane FP and DFB lasers for the 3QW active region. As can be seen, the stripe structure with steps (solid lines) has a lower threshold current than a completely flat stripe structure (dashed lines), owing to the

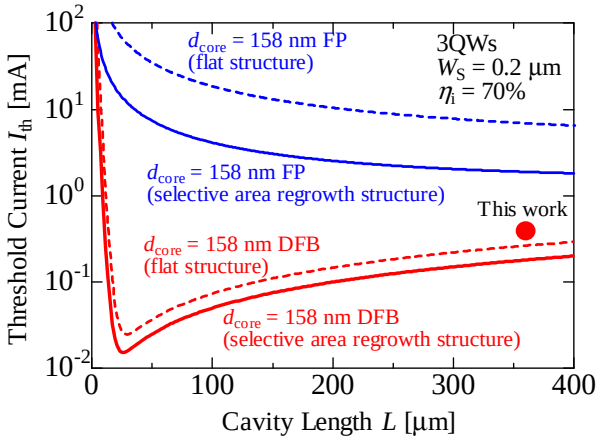

Fig. 6. (Color online) Dependence of theoretical threshold current on the cavity length for membrane FP and DFB lasers.

higher optical confinement factor into the active region. Although the measured threshold current 390 μA of the membrane DFB laser is slightly higher than the calculated value for the completely flat structure, it is much lower than that of membrane FP lasers. From this figure, we can expect an ultralow-threshold-current operation of approximately 15 μA, with a cavity length of 25 μm. These values are appropriate for use in on-chip optical interconnects.

In conclusion, we demonstrated a low-threshold-current operation of a 1.56-μm-wavelength membrane DFB laser with BCB bonding on a Si substrate. As a result, a threshold current of as low as 390 μA was obtained for a cavity length of 360 μm and a stripe width of 0.2 μm. Even though a clear single-mode operation was not observed, this low threshold property can be explained by the increased optical confinement factor of the active region, due to the formation of a slight step during the embedding growth of the InP cladding layers.

Acknowledgments The authors would like to thank Professors M. Asada, Y. Miyamoto, T. Mizumoto, and S. Akiba of the Tokyo Institute of Technology, Tokyo, Japan, for fruitful discussions. This work was supported by JSPS KAKENHI Grant Numbers 24246061, 25709026, 25420321, and 13J08092.

1) D. A. B. Miller, Proc. IEEE **97**, 1166 (2009).
2) P. Moser, W. Hofmann, P. Wolf, J. A. Lott, G. Larisch, A. Payusov, N. N. Ledentsov, and D. Bimberg, Appl. Phys. Lett. **98**, 231106 (2011).
3) S. Imai, K. Takaki, S. Kamiya, H. Shimizu, J. Yoshida, Y. Kawakita, T. Takagi, K. Hiraiwa, H. Shimizu, T. Suzuki, N. Iwai, T. Ishikawa, N. Tsukiji, and A. Kasukawa, IEEE J. Sel. Top. Quantum Electron. **17**, 1614 (2011).
4) S. Matsuo, A. Shinya, T. Kakitsuka, K. Nozaki, T. Segawa, T. Sato, and M. Notomi, Nat. Photonics **4**, 648 (2010).
5) B. Ellis, M. A. Mayer, G. Shambat, T. Sarmiento, J. Harris, E. E. Haller, and J. Vuckovic, Nat. Photonics **5**, 297 (2011).
6) S. Matsuo, T. Sato, K. Takeda, A. Shinya, K. Nozaki, H. Taniyama, M. Notomi, K. Hasebe, and T. Kakitsuka, IEEE J. Sel. Top. Quantum Electron. **19**, 4900311 (2013).
7) T. Okamoto, N. Nunoya, Y. Onodera, S. Tamura, and S. Arai, Electron. Lett. **38**, 1444 (2002).
8) T. Okamoto, N. Nunoya, Y. Onoda, T. Yamazaki, S. Tamura, and S. Arai, IEEE J. Sel. Top. Quantum Electron. **9**, 1361 (2003).
9) T. Okamoto, T. Yamazaki, S. Sakamoto, S. Tamura, and S. Arai, IEEE Photonics Technol. Lett. **16**, 1242 (2004).
10) S. Arai, N. Nishiyama, T. Maruyama, and T. Okumura, IEEE J. Sel. Top. Quantum Electron. **17**, 1381 (2011).
11) S. Sakamoto, H. Naitoh, M. Ohtake, Y. Nishimoto, S. Tamura, T. Maruyama, N. Nishiyama, and S. Arai, IEEE J. Sel. Top. Quantum Electron. **13**, 1135 (2007).
12) S. Sakamoto, H. Naitoh, M. Ohtake, Y. Nishimoto, T. Maruyama, N. Nishiyama, and S. Arai, Jpn. J. Appl. Phys. **46**, L1155 (2007).
13) K. Oe, Y. Noguchi, and C. Caneau, IEEE Photonics Technol. Lett. **6**, 479 (1994).
14) T. Okumura, M. Kurokawa, M. Shirao, D. Kondo, H. Ito, N. Nishiyama, T. Maruyama, and S. Arai, Opt. Express **17**, 12564 (2009).
15) T. Okumura, H. Ito, D. Kondo, N. Nishiyama, and S. Arai, Jpn. J. Appl. Phys. **49**, 040205 (2010).
16) T. Okumura, T. Koguchi, H. Ito, N. Nishiyama, and S. Arai, Appl. Phys. Express **4**, 042101 (2011).
17) T. Shindo, T. Okumura, H. Ito, T. Koguchi, D. Takahashi, Y. Atsumi, J. H. Kang, R. Osabe, T. Amemiya, N. Nishiyama, and S. Arai, Opt. Express **19**, 1884 (2011).
18) M. Futami, K. Shinno, T. Shindo, K. Doi, T. Amemiya, N. Nishiyama, and S. Arai, Proc. 1st Opt. Interconnects Conf., 2012, p. 34.
19) K. Doi, T. Shindo, M. Futami, J. Lee, T. Hiratani, D. Inoue, S. Yang, T. Amemiya, N. Nishiyama, and S. Arai, 25th Int. Conf. Indium Phosphide and Related Materials, 2013, We-D2-3.
20) D. Inoue, J. Lee, K. Doi, T. Hiratani, Y. Atsuji, T. Amemiya, N. Nishiyama, and S. Arai, Appl. Phys. Express **7**, 072701 (2014).
21) S. Matsuo, T. Fujii, K. Hasebe, K. Takeda, T. Sato, and T. Kakitsuka, Proc. European Conf. Optical Communication (ECOC), 2014, MO.4.4.3.
22) Y. Atsuji, K. Doi, J. Lee, Y. Atsumi, T. Hiratani, D. Inoue, T. Amemiya, N. Nishiyama, and S. Arai, 26th Int. Conf. Indium Phosphide and Related Materials, 2014, We-D2-2.
23) A. Sakai, G. Hara, and T. Baba, Jpn. J. Appl. Phys. **40**, L383 (2001).